

Phase diagram of V_2O_3 - Fe_tO - SiO_2 - CaO (15 mass%) system at 1623 K

Baijun Yan¹, Daya Wang², Tengfei Deng³, Bo Song¹ and Qifeng Shu⁴

1. Professor, School of Metallurgical and Ecological Engineering, University of Science and Technology Beijing, Beijing China 100083. Email: baijunyan@ustb.edu.cn
2. Senior researcher, Safety and Environmental Engineering Technology Institute, Sinosteel Group, Maanshan China 243071. Email: dayawangustb@126.com
3. Professor, State Key Laboratory of Silicate Materials for Architectures, Wuhan University of Technology, Wuhan China 430070. Email: dengtf@whut.edu.cn
4. Professor, Research Unit of Process Metallurgy, University of Oulu, Oulu Finland 90014. Email: qifeng.shu@oulu.fi

Keywords: Phase diagram, V-bearing oxide system, Phase equilibrium

ABSTRACT

In view of the lack of phase equilibria data of vanadium-bearing oxide system and the desirability of them for design or optimization of vanadium extraction process, the phase equilibria relationships of V_2O_3 -FeO-SiO₂-CaO(15 mass%) system were determined experimentally, and then an isothermal section phase diagram of this system was constructed. Totally, 81 samples of different composition were equilibrated at 1623 K for 48 hours in iron crucible under Ar atmosphere. The equilibrated samples were quenched quickly in cold water, and then the phase constituents of all the samples were identified by XRD combined with EPMA measurements. 17 different types of phase equilibria relationship were determined, by using L to represent liquid phase they are summarized and numbered as follows: 1) single L, 2) L + SiO₂, 3) L + spinel + SiO₂, 4) L + spinel + SiO₂ + (V,Fe)₂O₃, 5) L + SiO₂ + (V,Fe)₂O₃, 6) L + (Ca,Fe)₃V₂Si₃O₁₂ + SiO₂ + (V,Fe)₂O₃, 7) L + (V,Fe)₂O₃, 8) L + spinel + (V,Fe)₂O₃, 9) L + spinel + (Ca,Fe)₃V₂Si₃O₁₂ + (V,Fe)₂O₃, 10) L + (Ca,Fe)₃V₂Si₃O₁₂ + (V,Fe)₂O₃, 11) spinel + (Ca,Fe)₃V₂Si₃O₁₂ + (V,Fe)₂O₃, 12) (Ca,Fe)₃V₂Si₃O₁₂ + (V,Fe)₂O₃, 13) L + Fe_tO + (V,Fe)₂O₃, 14) L + spinel, 15) L + Fe_tO, 16) L + spinel + (Ca,Fe)₃V₂Si₃O₁₂, and 17) L + SiO₂ + (Ca,Fe)₃V₂Si₃O₁₂. Finally, based on the measured experimental data and the neighboring phase field rule, the sectional diagram of V_2O_3 -FeO-SiO₂-CaO(15 mass%) system at 1623 K composed of 17 phase equilibria areas was presented.

1. INTRODUCTION

Vanadium is an important transition metal element, which has been widely used in many areas, such as catalysis, electrode materials and laser materials etc (Du et al.,2018; Ejigu et al.,2015; Tomashchuk et al.,2015). In the vanadium industry, about 80% of the vanadium is extracted from the vanadium-bearing ores, while the reminder comes from the secondary sources including residues and ashes from the petroleum industry, and recycled spent catalysts (Dai et al.,2012; Ketris et al.,2009). Of the production of vanadium by ores, the most commonly used ores are vanadium-titanium magnetite and vanadium-bearing black shale (Dai et al.,2018).

As for the extraction of vanadium from the vanadium-titanium magnetite, it is firstly smelted and reduced in blast furnace to obtain vanadium-bearing hot metal (Smirnov et al.,2010). Then, the vanadium-bearing hot metal is oxidized in converter to transfer and concentrate the vanadium to slag which is mainly constituted of iron oxide, silica and vanadium oxide (Fang et al.,2012; Dong et al.,2021). Next, the vanadium rich slag is adopted as feedstock for production of vanadium. In this vanadium rich slag, the vanadium mainly occurs in a spinel solid solution phase with iron vanadate ($Fe_{3-x}V_xO_4$) as its parent mineral. To raise the recovery rate of vanadium from the hot metal, the conditions favourable to the formation of the spinel phase are desired in practice. As the basis of optimization of the conditions, the thermodynamics of the SiO₂-Fe_tO-V₂O₃ system are essential.

Regarding the extraction of vanadium from the black shale, which is mainly composed of SiO₂, CaO, Al₂O₃, MgO and small amounts of V₂O₃, Fe_tO etc., the general process of vanadium extraction is direct soda roasting followed by leaching. However, due to the very low vanadium content in the shale, this process is faced with the environmental issues such as large production of effluent in leaching, high energy and soda consumption at roasting, etc (Seredin et al.,2012; Chen et al.,2014). To improve the vanadium grade, a novel beneficiation method of vanadium was developed by our group (Yan et al.,2018; Wang et al.,2019A). Where, Fe₂O₃ is added to the shale, and the vanadium occurred in shale is transformed into $Fe_{3-x}V_xO_4$ spinel phase by reducing roast. Then, the formed $Fe_{3-x}V_xO_4$ spinel phase is separated by magnetic method, and the acquired high-grade vanadium concentrate is used as feedstock for extraction of vanadium. To optimize the conditions and ensure the formation of $Fe_{3-x}V_xO_4$ spinel phase effectively, the thermodynamics of the CaO-SiO₂-Fe_tO-V₂O₃ system is required basically (Yan et al.,2020A; Yan et al.,2020B; Wang et al.,2019B; Wang et al.,2017).

In addition, the solid solution $Fe_{3-x}V_xO_4$ spinel phase possesses versatile properties and is with broad potential applications, its preparation also needs the related thermodynamic information as guideline. However, the thermodynamic studies on the oxide system containing both vanadium oxide and iron oxide are scarce and insufficient. Huang et al. (Huang et al.,2016) calculated a phase diagram of FeO-SiO₂-V₂O₃ system on base of the binary subsystem by using the FactSage software. But, due to the lack of the thermodynamic data of the $Fe_{3-x}V_xO_4$ spinel phase, they can only use the stoichiometric compound FeV₂O₄ to substitute for $Fe_{3-x}V_xO_4$. This replacement definitely brings about

a large uncertainty on the calculated phase diagram. Semykina et al. (Semykina et al.,2012) reported that vanadium ferrites (FeV_2O_4 and Fe_2VO_4) can be formed in $\text{CaO-SiO}_2\text{-FeO-V}_2\text{O}_5$ system at 1773 K in argon atmosphere. Li et al. (Li et al.,2019) investigated the effect of CaO addition on the evolution of main phases in the $\text{Fe-Fe}_2\text{O}_3\text{-V}_2\text{O}_3$ system under argon atmosphere, but in alike manner, they treated the spinel solid solution phase as stoichiometric compound Fe_2VO_4 . Fang et al. (Fang et al.,2015) investigated the influence of CaO on the occurrence state of vanadium in slag, and pointed out that with the increasing of CaO content the vanadium-bearing spinel phase transforms into goldmanite $\text{Ca}_3\text{V}_2(\text{SiO}_4)_3$ phase gradually.

From the above summarization, it can be seen that the phase relations of the silicate system containing both vanadium oxide and iron oxide are interesting and important, whereas the available studies are not only scrappy but also deficient. Therefore, in the present study, the phase relations in the $\text{CaO}(15 \text{ mass}\%)\text{-SiO}_2\text{-Fe}_t\text{O-V}_2\text{O}_3$ system were investigated systematically at 1623 K, and an isothermal phase diagram of the system was constructed.

2. EXPERIMENTAL

2.1 Determination of experimental conditions

To get a correct phase diagram of a high-order system, it is crucial to choose correct variables which are adopted as the axes of the diagram. For a N -component system, due to the Gibbs-Duhem relation shown as Eq. (1), only $N+1$ potential variables of T , P and μ_i are independent.

$$SdT - VdP + \sum N_i d\mu_i = 0 \quad (1)$$

Where, S , V and N_i are extensive variables representing the entropy, volume and the content of component i , respectively. T , P and μ_i are conjugate potentials of S , V and N_i , representing temperature, pressure and chemical potential of component i respectively.

As for the variables, which can be adopted as the axes of a phase diagram, a general way to determined them is as follows. For example, for a N -component system. Firstly, n potentials from the Gibbs-Duhem relation, $n \leq N+1$, are chosen, and these potentials are denoted as $\varphi_1, \varphi_2, \dots, \varphi_n$. Secondly, from the remaining conjugate pairs, the variables N_i are used to form $(N+1-n)$ independent ratios, which are denoted as $Q_{n+1}, Q_{n+2}, \dots, Q_{N+1}$. The formula to form Q_i is shown as Eq. (2).

$$Q_i = N_i / \sum_{j=n+1}^{N+1} N_j \quad (n + 1 \leq i \leq N + 1) \quad (2)$$

Thirdly, a set of $(N+1)$ independent variables $\varphi_1, \varphi_2, \dots, \varphi_n, Q_{n+1}, Q_{n+2}, \dots, Q_{N+1}$ is formed. Finally, any two variables in this set can be selected and the remainder are held constant to construct a true two-dimensional phase diagram.

In the present study, the following set of variables was formed: T , P , μ_{Fe} , $N_{\text{CaO}} / (N_{\text{SiO}_2} + N_{\text{V}_2\text{O}_3} + N_{\text{FeO}} + N_{\text{CaO}})$, $N_{\text{SiO}_2} / (N_{\text{SiO}_2} + N_{\text{V}_2\text{O}_3} + N_{\text{FeO}} + N_{\text{CaO}})$, and $N_{\text{V}_2\text{O}_3} / (N_{\text{SiO}_2} + N_{\text{V}_2\text{O}_3} + N_{\text{FeO}} + N_{\text{CaO}})$. To construct a two-dimension phase diagram, the temperature was fixed at 1623 K, the pressure was fixed by equilibrating the sample in Ar atmosphere of 1 atm, the μ_{Fe} was fixed by using pure Fe crucible to contain the sample, and $N_{\text{CaO}} / (N_{\text{SiO}_2} + N_{\text{V}_2\text{O}_3} + N_{\text{FeO}} + N_{\text{CaO}})$ was fixed to be 15 mass pct. Then, the phase relationships of the system with various contents of SiO_2 , V_2O_3 and FeO were measured, and a Gibbs triangle representing the compositions of SiO_2 , V_2O_3 and FeO was adopted to demonstrate the measured phase relationships.

2.2 Materials and sample preparation

The chemical agents CaO , SiO_2 and V_2O_3 with purity higher than 99.9 mass% were used as reactants. Before weighing, CaO and SiO_2 were dried at 1273K in air for 24 hours. FeO was prepared by using chemical agents Fe_2O_3 and Fe as the raw materials. The powders of Fe_2O_3 and Fe with molar ratio of 1 were mixed homogeneously and pressed into tablets, then the tablets were heated at 1323 K in the atmosphere of $\text{CO/CO}_2=1$ for 48 hours.

Afterwards, about 1g mixture of the four oxides were homogenized in an agate mortar and pressed into a tablet, and then the tablet was placed into a pure iron crucible (10-mm O.D., 9-mm I.D., 30-mm height) for high-temperature equilibrium.

2.3 Procedure of equilibration

A vertical-tube resistance furnace heated by MoSi₂ elements was used for the equilibration, and the detailed description of this furnace can be found in a previous publication (Fang et al., 2015). The temperature of the furnace was controlled by a proportional-integral-differential (PID) controller with an accuracy of ±1 K. The temperature of the sample was measured by a W-Re5/W-Re26 thermocouple positioned just beneath the bottom of the alumina crucible. The atmospheres used was pure Ar with purity higher than 99.999%.

After the crucible containing the samples was hung in the even temperature zone of the furnace, the reaction chamber was sealed, evacuated and filled with Ar. Thereafter, the furnace was heated up at a rate of 3K/min to 1623K, and the flow rate of Ar was 100 mL/min. According to the results of the pre-experiments, the equilibration time was chosen to be 48 hours. When the equilibration was completed, the samples were lifted from the even temperature zone to the water quenching chamber and cooled quickly in the pure Ar reaction atmosphere. The samples were not taken out from Fe crucibles, the sample and the crucible together were mounted and polished.

2.4 Characterization of quenched samples

To identify the phases existed in the quenched samples, XRD measurement of the ground powder sample was performed firstly. A Bruker D8-Advance X-ray powder diffractometer with Cu K α radiation ($\lambda = 1.5406 \text{ \AA}$) (Bruker AXS, Germany) was used, and the scattering angles was from 10° to 90°. Then, to determine the composition of the equilibrated phases, SEM-EPMA measurements were performed. A JEOL JXL-8230 instrument with wavelength dispersive spectrometers was adopted. The measurements were conducted with an accelerating voltage of 20 kV, a beam current of 10 nA, and a spot size of nearly 1 μm . Fe₂O₃, CaSO₄, NaAlSi₃O₈ and V-P-Pb glass (V₂O₅: 59.82%, P₂O₅: 29.55%, PbO: 11.50%) were used as the standards for the quantitative analysis of Fe, Ca, Si and V in each mineral phase.

3. RESULTS AND DISCUSSION

3.1 Phase relations of V₂O₃-FeO-SiO₂-CaO(15 mass %) system at 1623 K

Totally, 81 samples with different composition were equilibrated at 1623 K under Ar atmosphere. All the equilibrated-quenched samples were observed by SEM, it could be found from the back-scattered electrons micrograph that the microstructures of the quenched sample are composed of matrix and crystal phases. The matrix comes from the liquid phase in the equilibrated sample, which was super cooled in the process of quenching and formed the amorphous matrix. The crystal phase is the solid phase that is in equilibrium with the liquid phase at 1623 K, and the crystal phases were further identified by XRD.

From the combining measurements of SEM-EPMA and XRD, it can be found that, beside the liquid phase, five crystal phases can be found in the investigated samples. These five crystal phases are SiO₂, (V,Fe)₂O₃, Fe_{3-x}V_xO₄, Fe₂O and (Ca,Fe)₃V₂Si₃O₁₂. The Fe crucibles were adopted and the solid Fe phase must have been present in the sample. As for the phase equilibria relationships of these crystal phases and the liquid phase, totally 15 different phase equilibria relationships were found in the examined samples. The 15 phase equilibria relationships included one single-phase area of liquid, four two-phase areas of coexisting between solid and liquid, five three-phase areas of coexisting among two solids and liquid, three four-phase areas of coexisting among three solids and liquid, and two areas of coexisting only solid phases. The detailed information of the found 15 phase equilibria relations are shown in Table 1.

Table 1 The phase equilibria relations in CaO(15 mass%)-SiO₂-Fe₂O-V₂O₃ at 1623 K

Coexisting phase	Phase equilibria relations
Single-liquid (one area)	L

Two-phase coexisting (four areas)	L+Tridymite(SiO_2),L+Wüstite(Fe_tO), L+Karelianite($(\text{V,Fe})_2\text{O}_3$), L+Spinel($\text{Fe}_{3-x}\text{V}_x\text{O}_4$)
Three-phase coexisting (five areas)	L+Spinel($\text{Fe}_{3-x}\text{V}_x\text{O}_4$)+Tridymite(SiO_2), L+Spinel($\text{Fe}_{3-x}\text{V}_x\text{O}_4$)+Karelianite($(\text{V,Fe})_2\text{O}_3$), L+Tridymite(SiO_2)+Karelianite($(\text{V,Fe})_2\text{O}_3$), L+(Ca,Fe) $_3\text{V}_2\text{Si}_3\text{O}_{12}$ + Karelianite($(\text{V,Fe})_2\text{O}_3$), L+ Spinel($\text{Fe}_{3-x}\text{V}_x\text{O}_4$)+Wüstite(Fe_tO)
Four-phase coexisting (three areas)	L+Spinel($\text{Fe}_{3-x}\text{V}_x\text{O}_4$)+Tridymite(SiO_2)+Karelianite($(\text{V,Fe})_2\text{O}_3$), L+Spinel($\text{Fe}_{3-x}\text{V}_x\text{O}_4$)+(Ca,Fe) $_3\text{V}_2\text{Si}_3\text{O}_{12}$ +Karelianite($(\text{V,Fe})_2\text{O}_3$), L+ (Ca,Fe) $_3\text{V}_2\text{Si}_3\text{O}_{12}$ +Karelianite($(\text{V,Fe})_2\text{O}_3$)+ Tridymite(SiO_2)
only solid phases coexisting (two areas)	Spinel ($\text{Fe}_{3-x}\text{V}_x\text{O}_4$)+(Ca,Fe) $_3\text{V}_2\text{Si}_3\text{O}_{12}$ +Karelianite($(\text{V,Fe})_2\text{O}_3$), (Ca,Fe) $_3\text{V}_2\text{Si}_3\text{O}_{12}$ +Karelianite($(\text{V,Fe})_2\text{O}_3$)

The SEM micrograph and the XRD patterns of the investigated samples are shown according to the phase equilibria relationships.

3.1.1 Single liquid

At 1623 K, there was one single-liquid area in the CaO (15 mass%)- SiO_2 - Fe_tO - VO_x system. The typical backscattered electron image and XRD pattern of the single-liquid sample are shown in Figure 1(a) and (b), respectively.

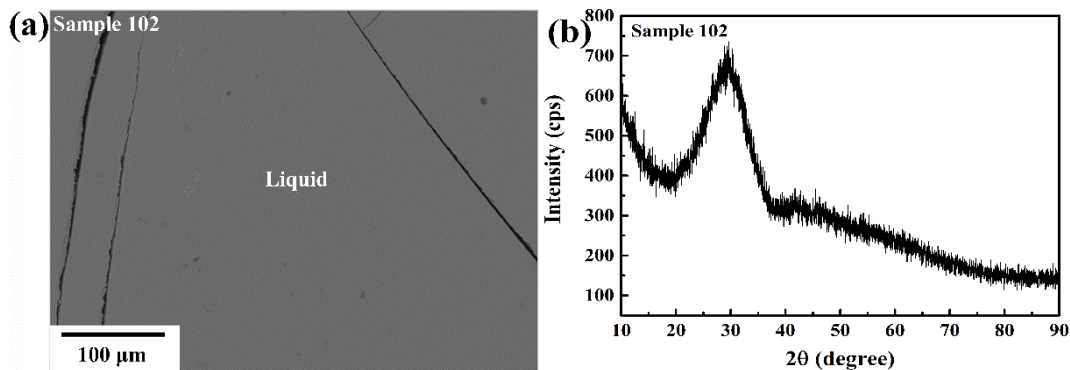


Figure 1 The backscattered electron image (a) and XRD pattern (b) of single-liquid sample

3.1.2 Coexisting of one solid phase and liquid

The typical backscattered electron image and XRD pattern of the sample containing one solid phase and one liquid phase simultaneously are shown in Figure 2 through 5. In Figure 2, that of the sample containing SiO_2 and liquid are presented. Figure 3 is for the case of coexisting between spinel phase ($\text{Fe}_{3-x}\text{V}_x\text{O}_4$) and liquid, Figure 4 for coexisting between Wüstite (Fe_tO) and liquid, Figure 5 for coexisting between Karelianite($(\text{V,Fe})_2\text{O}_3$) and liquid.

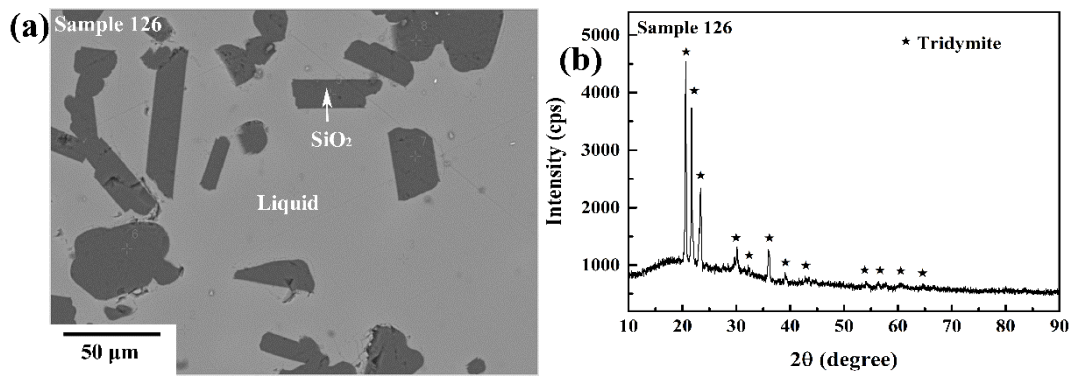


Figure 2 Backscattered electron image (a) and XRD pattern (b) of SiO₂-liquid coexisting sample

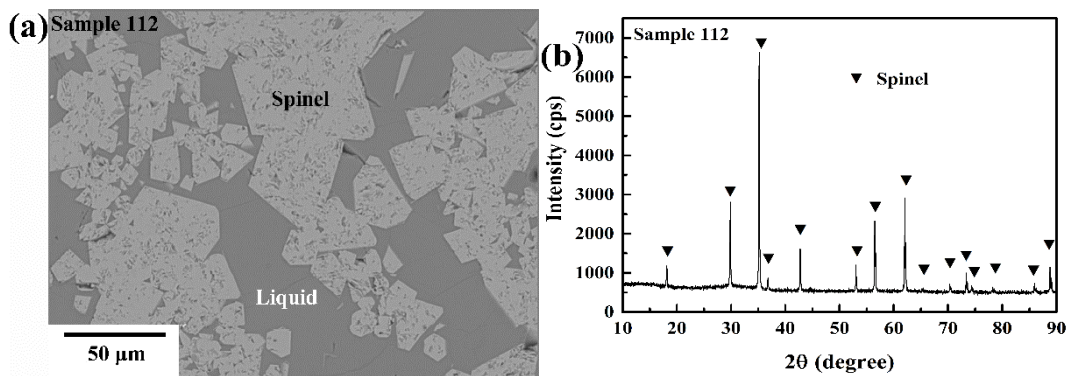


Figure 3 Backscattered electron image (a) and XRD pattern (b) of Fe_{3-x}V_xO₄-liquid coexisting sample

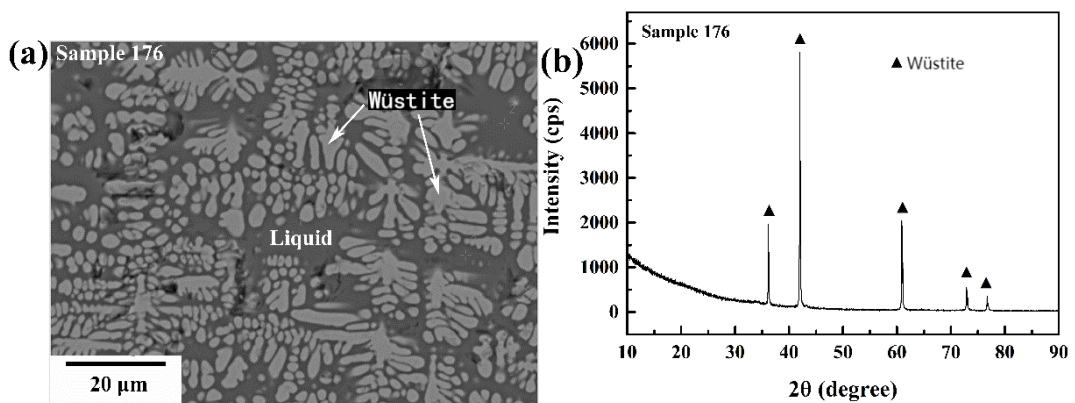


Figure 4 Backscattered electron image (a) and XRD pattern (b) of Fe_TO-liquid coexisting sample

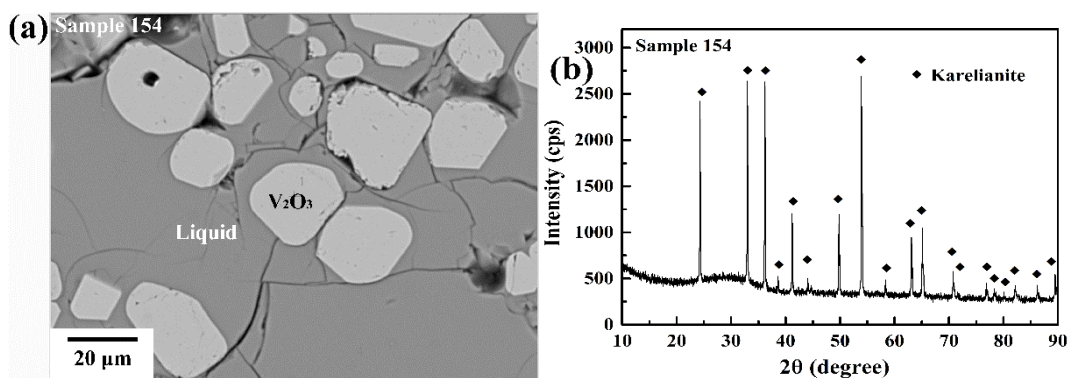


Figure 5 Backscattered electron image (a) and XRD pattern (b) of (V,Fe)₂O₃-liquid coexisting sample

3.1.3 Coexisting of two solid phases and liquid

Among the investigated samples, five cases of coexisting between two solid phases and liquid were found. The micrograph and the XRD patterns of the representative samples were shown in Figure 6 through 10.

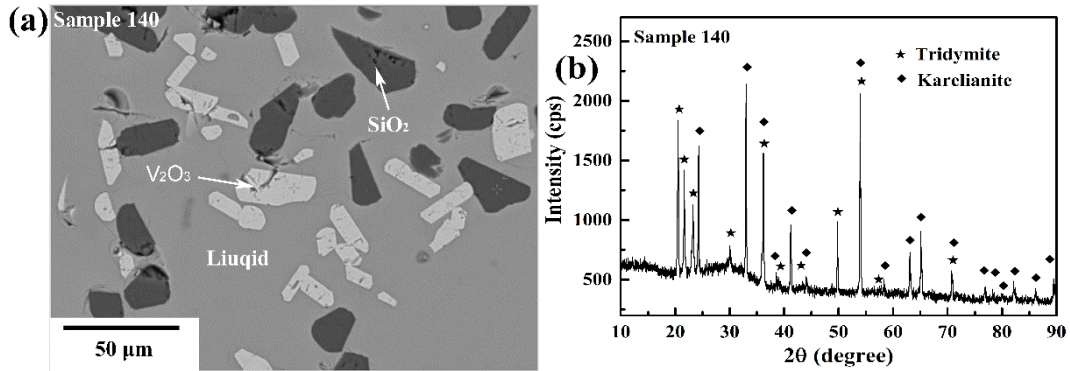


Figure 6 Backscattered electron image (a) and XRD pattern (b) of $(\text{V,Fe})_2\text{O}_3$ - SiO_2 -liquid coexisting sample

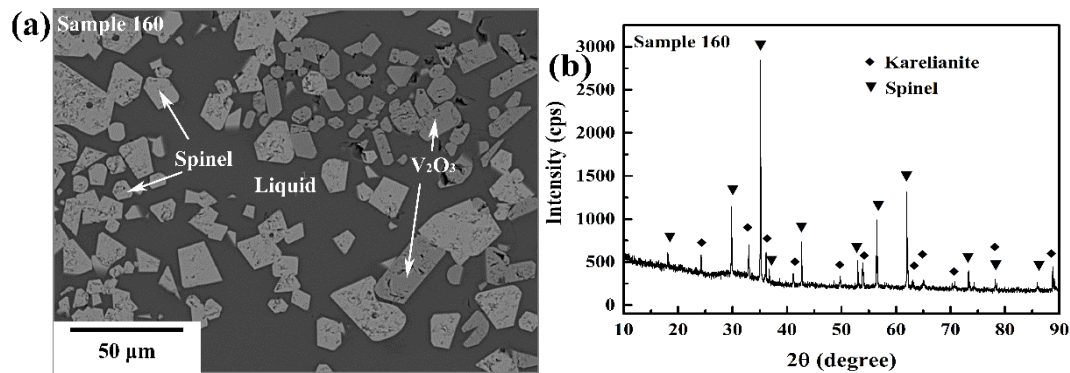


Figure 7 Backscattered electron image (a) and XRD pattern (b) of $(\text{V,Fe})_2\text{O}_3$ - $\text{Fe}_{3-x}\text{V}_x\text{O}_4$ -liquid coexisting sample

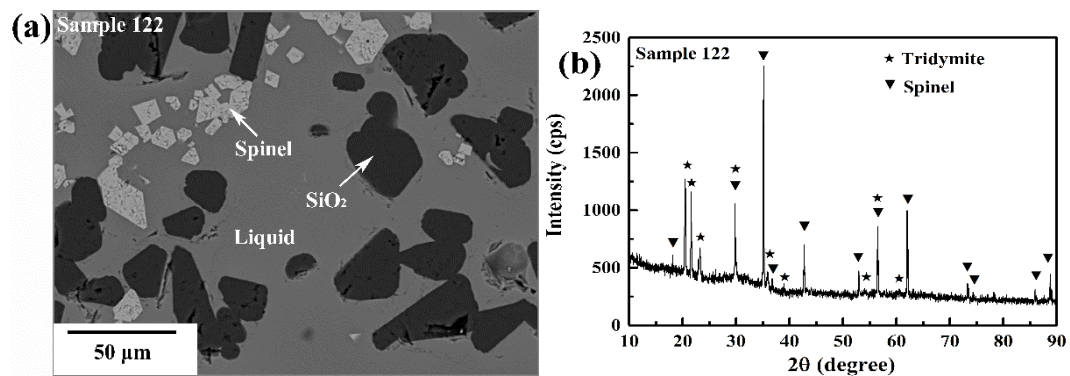


Figure 8 Backscattered electron image (a) and XRD pattern (b) of SiO_2 - $\text{Fe}_{3-x}\text{V}_x\text{O}_4$ -liquid coexisting sample

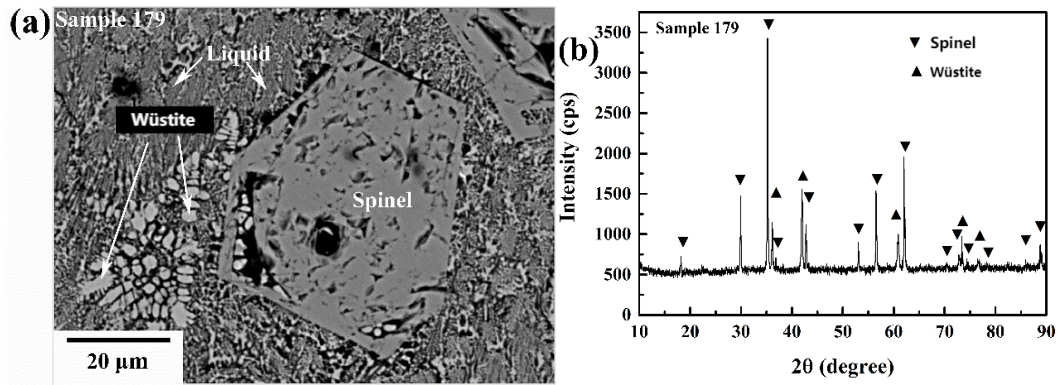


Figure 9 Backscattered electron image (a) and XRD pattern (b) of $\text{Fe}_3\text{O}-\text{Fe}_{3-x}\text{V}_x\text{O}_4$ -liquid coexisting sample

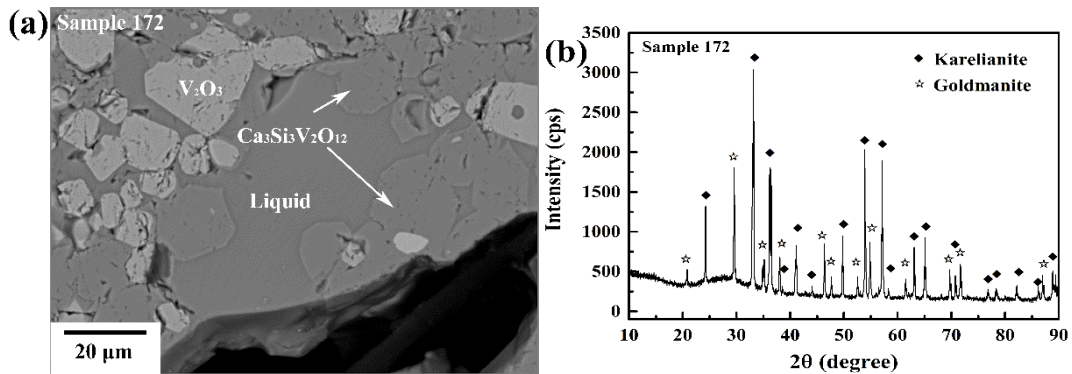


Figure 10 Backscattered electron image (a) and XRD pattern (b) of $(\text{V,Fe})_2\text{O}_3$ - $(\text{Ca,Fe})_3\text{V}_2\text{Si}_3\text{O}_{12}$ -liquid coexisting sample

3.1.4 Coexisting of three solid phases and liquid

Three different four-phase equilibria were found in the investigated sample. One is liquid phase equilibrating with solid phases SiO_2 , $(\text{V,Fe})_2\text{O}_3$ and $(\text{Ca,Fe})_3\text{V}_2\text{Si}_3\text{O}_{12}$, as shown in Figure 11. The second is liquid phase equilibrating with solid phases SiO_2 , $(\text{V,Fe})_2\text{O}_3$ and $\text{Fe}_{3-x}\text{V}_x\text{O}_4$, as shown in Figure 12. The third is liquid phase equilibrating with solid phases $(\text{Ca,Fe})_3\text{V}_2\text{Si}_3\text{O}_{12}$, $(\text{V,Fe})_2\text{O}_3$ and $\text{Fe}_{3-x}\text{V}_x\text{O}_4$, as shown in Figure 13.

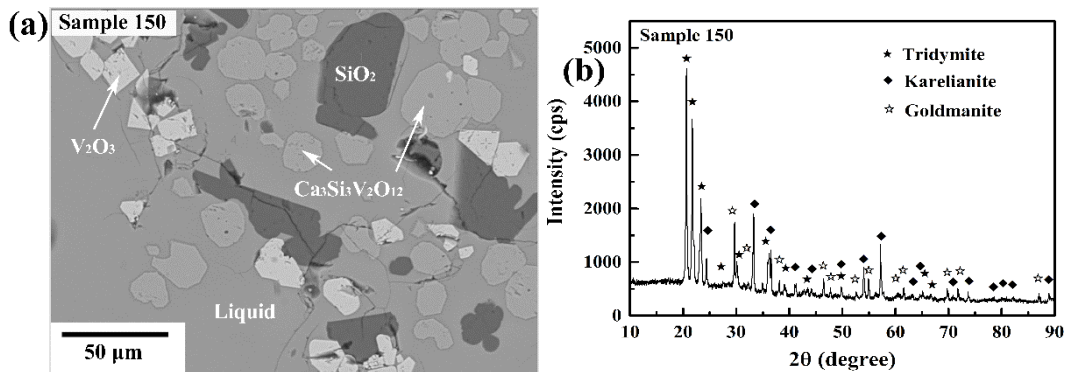


Figure 11 Backscattered electron image (a) and XRD pattern (b) of $(\text{V,Fe})_2\text{O}_3$ - $(\text{Ca,Fe})_3\text{V}_2\text{Si}_3\text{O}_{12}$ - SiO_2 -liquid coexisting sample

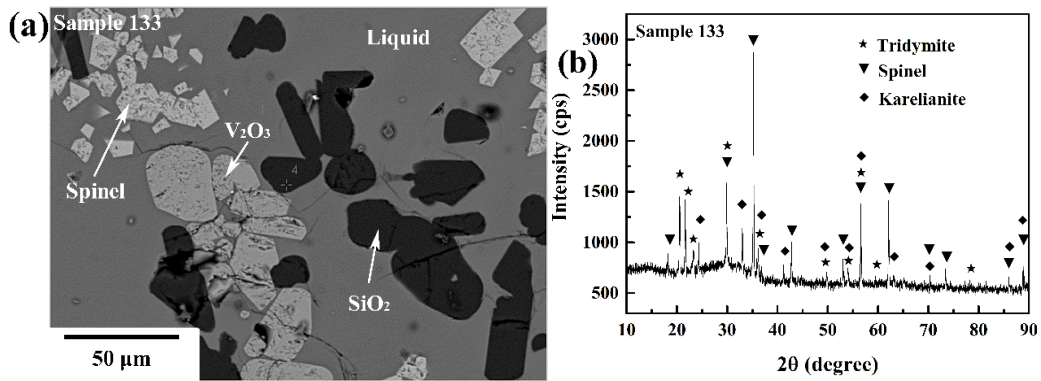


Figure 12 Backscattered electron image (a) and XRD pattern (b) of $(V,Fe)_2O_3$ - $Fe_{3-x}V_xO_4$ - SiO_2 -liquid coexisting sample

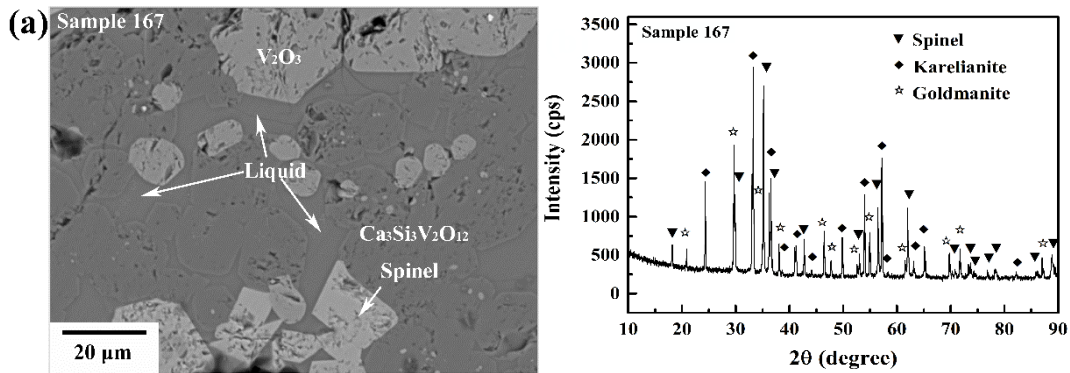


Figure 13 Backscattered electron image (a) and XRD pattern (b) of $(V,Fe)_2O_3$ - $(Ca,Fe)_3V_2Si_3O_{12}$ - $Fe_{3-x}V_xO_4$ - SiO_2 -liquid coexisting sample

3.1.5 Coexisting only solid phases

Two different solid-phase equilibria were found in the investigated sample. One is equilibrium among three solid phases, Goldmanite($(Ca,Fe)_3V_2Si_3O_{12}$), Kareljanite($(V,Fe)_2O_3$) and Spinel($Fe_{3-x}V_xO_4$), as shown in Figure 14. The other is equilibrium between Goldmanite($(Ca,Fe)_3V_2Si_3O_{12}$) and Kareljanite($(V,Fe)_2O_3$), as shown in Figure 15.

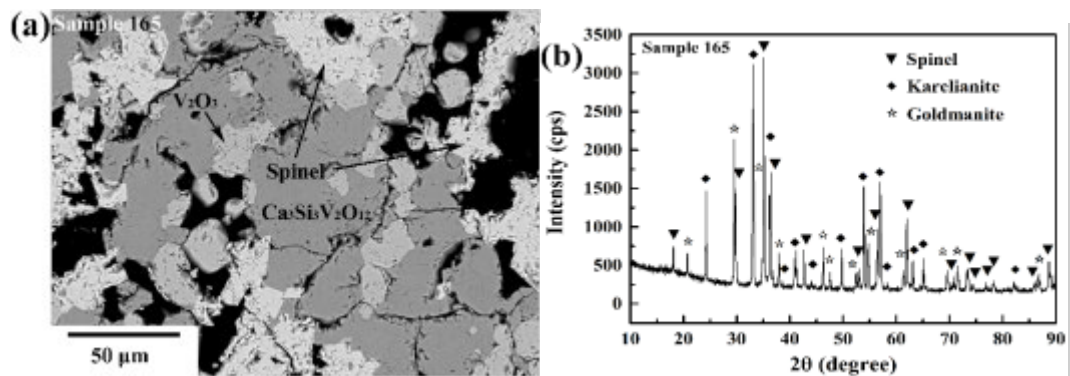


Figure 14 Backscattered electron image (a) and XRD pattern (b) of $(V,Fe)_2O_3$ - $(Ca,Fe)_3V_2Si_3O_{12}$ - $Fe_{3-x}V_xO_4$ coexisting sample

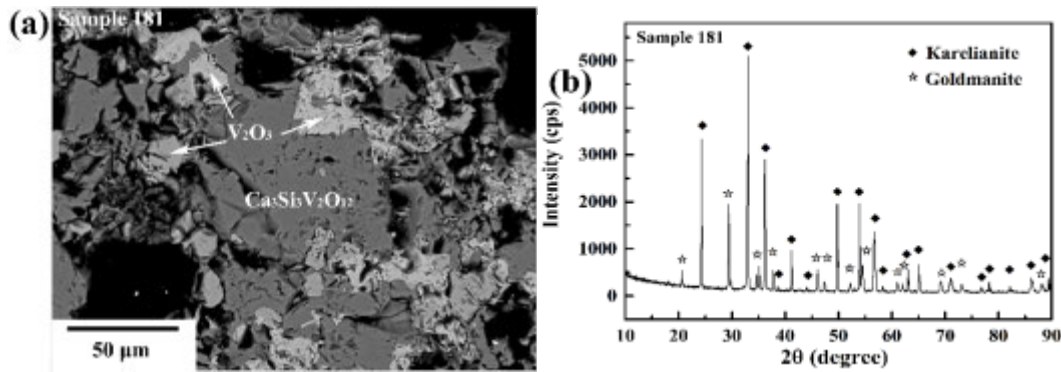


Figure 15 Backscattered electron image (a) and XRD pattern (b) of $(V,Fe)_2O_3$ - $(Ca,Fe)_3V_2Si_3O_{12}$ coexisting sample

3.2 Phase diagram of V_2O_3 -FeO-SiO₂-CaO(15 mass %) system at 1623 K

Based on the above-determined phase equilibria relationships, the iso-sectional phase diagram of V_2O_3 -Fe_tO-SiO₂-CaO(15 mass%) system at 1623 K was constructed, which is shown in Figure 16.

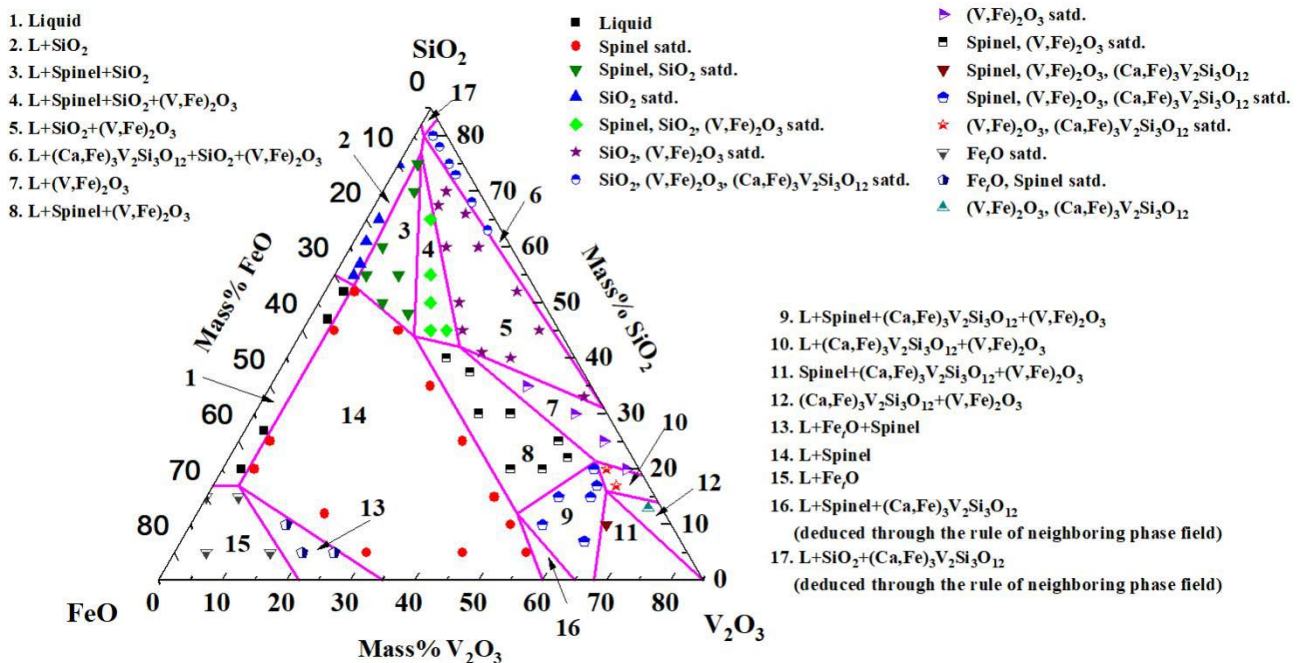


Figure 16 The iso-sectional phase diagram of V_2O_3 -Fe_tO-SiO₂-CaO(15 mass%) system at 1623 K

In Figure 16, all the symbols such as the solid star, solid triangle, solid square etc. represent the investigated samples, their positions represent the compositions of the samples, and different symbols represent different phase constituents. For example, the red solid circle symbols represent the samples which were constituted of spinel phase and liquid phase. According to the change of the phase constituents of the samples, the phase boundaries of different phase fields, which are lines in the two-dimensional phase diagram, were determined. Finally, the V_2O_3 -Fe_tO-SiO₂-CaO(15 mass%) system was segmentalized into 17 areas, and the areas were numbered from 1 to 17. The phase constituents of each phase field was also provided in Figure 16.

In Figure 16, it can also be seen that four linear phase boundaries meet at a point, which is the smaller unit composing the whole phase diagram. For each smaller unit, it was indicated by Mats Hillert (Hillert et al., 2008) that the numbers of phases in the phase fields around the intersection point have the relations as shown in Figure 17.

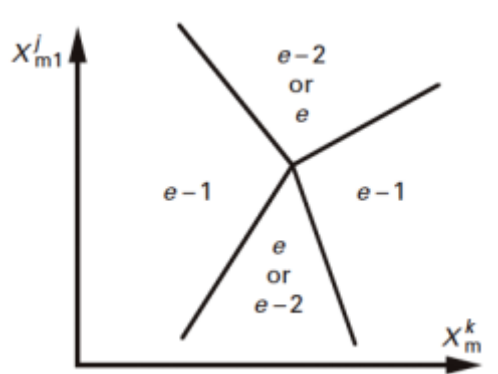


Figure 17 Elementary unit of a molar phase diagram, the e values from 3 to a maximum determined by the number of sectioning.

As mentioned above, totally 17 phase fields were indicated in Figure 16. However, only 15 different phase equilibria relationships were determined experimentally. For the un-experimentally determined phase fields 16 and 17, they were deduced according to the rule of neighboring phase field as shown in Figure 17. So, the phase constituents in the phase fields 16 and 17 should be confirmed by experiments in future.

4. CONCLUSIONS

In the present study, the traditional method of high temperature equilibration followed by quenching and combination of SEM and XRD measurements was adopted to identify the phase constituents of the samples. Then, based on the experimentally determined phase equilibria relationships, the isosectional phase diagram of V_2O_3 - Fe_tO - SiO_2 - CaO (15 mass%) system at 1623 K was constructed. The results revealed that the phase diagram is composed of 17 phase fields. The 17 phase fields are as follows: 1) single Liquid, 2) Liquid + SiO_2 , 3) Liquid + spinel + SiO_2 , 4) Liquid + spinel + SiO_2 + $(V,Fe)_2O_3$, 5) Liquid + SiO_2 + $(V,Fe)_2O_3$, 6) Liquid + $(Ca,Fe)_3V_2Si_3O_{12}$ + SiO_2 + $(V,Fe)_2O_3$, 7) Liquid + $(V,Fe)_2O_3$, 8) Liquid + spinel + $(V,Fe)_2O_3$, 9) Liquid + spinel + $(Ca,Fe)_3V_2Si_3O_{12}$ + $(V,Fe)_2O_3$, 10) Liquid + $(Ca,Fe)_3V_2Si_3O_{12}$ + $(V,Fe)_2O_3$, 11) spinel + $(Ca,Fe)_3V_2Si_3O_{12}$ + $(V,Fe)_2O_3$, 12) $(Ca,Fe)_3V_2Si_3O_{12}$ + $(V,Fe)_2O_3$, 13) Liquid + Fe_tO + $(V,Fe)_2O_3$, 14) Liquid + spinel, 15) Liquid + Fe_tO , 16) L + spinel + $(Ca,Fe)_3V_2Si_3O_{12}$, and 17) L + SiO_2 + $(Ca,Fe)_3V_2Si_3O_{12}$.

ACKNOWLEDGEMENTS

The financial support from National Natural Science Foundation of China on the projects of 51534001 and 52174274 were gratefully acknowledged.

REFERENCES

- Chen, J, Liu, G, Kang, Y, Wu, B, Sun, R, Zhou, C and Wu, D, 2014. Coal utilization in China: Environmental impacts and human health, *Environmental Geochemistry and Health*, 36(4):735-753.
- Dai, S, Ren, D, Chou, C-L, Finkelman, R B, Seredin, V V and Zhou, Y, 2012. Geochemistry of trace elements in Chinese coals: A review of abundances, genetic types, impacts on human health, and industrial utilization, *International Journal of Coal Geology*, 94(3-21).
- Dai, S, Zheng, X, Wang, X, Finkelman, R B, Jiang, Y, Ren, D, Yan, X and Zhou, Y, 2018. Stone coal in China: a review, *International Geology Review*, 60(5-6):736-753.
- Dong, Z H, Zhang, J and Yan, B J, 2021. Co-extraction of Vanadium Titanium and Chromium from Vanadium Slag by Oxalic Acid Hydrothermal Leaching with Synergy of Fe Powder, *Metallurgical and Materials Transactions B-Process Metallurgy and Materials Processing Science*, 52(6):3961-3969.
- Du, X, Xue, J, Wang, X, Chen, Y, Ran, J and Zhang, L, 2018. Oxidation of Sulfur Dioxide over V_2O_5/TiO_2 Catalyst with Low Vanadium Loading: A Theoretical Study, *The Journal of Physical Chemistry C*, 122(8):4517-4523.
- Ejigu, A, Edwards, M and Walsh, D A, 2015. Synergistic Catalyst-Support Interactions in a Graphene- Mn_3O_4 Electrocatalyst for Vanadium Redox Flow Batteries, *ACS Catalysis*, 5(12):7122-7130.
- Fang, H X, Li, H Y, Zhang, T, Liu, B-S and Xie, B, 2015. Influence of CaO on Existence form of Vanadium-containing Phase in Vanadium Slag, *ISIJ International*, 55(1):200-206.

- Fang, H X, Li, H Y and Xie, B,2012. Effective Chromium Extraction from Chromium-containing Vanadium Slag by Sodium Roasting and Water Leaching, *Isij International*,52(11):1958-1965.
- HILLERT, M, 2008. Phase Equilibria, Phase Diagrams and Phase Transformations,(Cambridge University Press: New York)
- Huang, W, Chen, M, Shen, X, Yu, S, Wang, N and Xu, L,2016. Phase Diagrams and Thermodynamic Properties of the FeO–SiO₂–V₂O₃ Systems, *steel research international*,88(6).
- Ketris, M P and Yudovich, Y E,2009. Estimations of Clarkes for Carbonaceous biolithes: World averages for trace element contents in black shales and coals, *International Journal of Coal Geology*,78(2):135-148.
- Li, X, Meng, F, Dong, X, Liang, D, Gao, F and Wei, Y,2019. Effect of CaO addition on phase formation in the Fe-Fe₂O₃-V₂O₃ system, *Journal of Alloys and Compounds*,772:955-960.
- Semykina, A, Dzhebian, I and Shatokha, V,2012. On the Formation of Vanadium Ferrites in CaO–SiO₂–FeO–V₂O₅ Slags, *steel research international*,83(12):1129-1134.
- Seredin, V V,2012. From coal science to metal production and environmental protection: A new story of success, *International Journal of Coal Geology*,90-91:1-3.
- Smirnov, L A, Filatov, S V and Rovnushkin, V A,2010. Removal of vanadium from low-silicon hot metal, *Steel Transl.*,40.
- Tomashchuk, I, Grevey, D and Sallamand, P,2015. Dissimilar laser welding of AISI 316L stainless steel to Ti6–Al4–6V alloy via pure vanadium interlayer, *Materials Science and Engineering: A*,622:37-45.
- Wang, D, Li, F and Yan, B,2019. Synthetic mechanism and kinetics of Fe₂VO₄ at 1273–1473 K from Fe₂O₃ and V₂O₃ under reducing atmosphere, *Journal of Alloys and Compounds*,797:1050-1058.
- Wang, D, Shu, Q, Yan, B, Wu, L, Wang, J and Dong, Y,2017. Thermodynamics of the CaO–SiO₂–VO_x system at 1873 K under the oxygen partial pressure of 6.9×10⁻¹¹ atm, *Journal of the American Ceramic Society*,100(10):4912-4927.
- Wang, D and Yan, B (2019). A Novel Approach for Pre-concentrating Vanadium from Stone Coal. Rare Metal Technology 2019, Cham, Springer International Publishing.
- Yan, B, Wang, D, Deng, T, Wu, L and Dong, Y,2020. Effects of oxygen partial pressure on the thermodynamics of CaO–SiO₂–VO_x system at 1873 K, *Journal of the American Ceramic Society*,103(3):2114-2127.
- Yan, B, Wang, D, Qiu, Q and Deng, T,2020. Phase relations in the “FeO–V₂O₃” system at 1473 K and the magnetic properties of spinel phase Fe_{3-x}V_xO₄, *Ceramics International*,46(5):6160-6167.
- Yan, B, Wang, D, Wu, L and Dong, Y,2018. A novel approach for pre-concentrating vanadium from stone coal ore, *Minerals Engineering*,125:231-238.